# Precision of 3-Configurations with Respective Sub-Configurations of 2-Ring Concentric Planar Array in Direction Finding

Kinyili, M. & Kitavi, D. M.

University of Embu, Kenya.

Correspondence: davismusyooo@gmail.com

#### **Abstract**

Direction finding is a key area of sensor array processing which is encountered in a broad range of important engineering applications. These applications include wireless communication, rada and sonar, among others. This work compares estimation accuracy of 3-configurations (based on the inner radius variation and constant outer radius) of a uniform 2-ring concentric planar array in direction finding via the Cramer-Rao bound derivation and analysis. The 3-configurations' estimation accuracy is articulated to their respective sub-configurations based on the sensors distribution in each ring. The sub-configurations use equal overall number of sensors (multiple of 4) but with 60% - 40% distribution, 50% - 50% distribution and 40% - 60% distribution on the inner-outer rings respectively. It is found that the estimation accuracy increases as the inner radius approaches the outer radius and thus configuration three (where the inner radius equals three-quarters of the outer radius) has the best precision in direction finding compared to configuration two (where the inner radius equals half of the outer radius) and configuration one (where the inner radius equals one-quarter of the outer radius). Furthermore, based on the subconfigurations (where there is varying sensor distribution along the two rings), sub-configuration three (where 40% of the sensors are distributed along the inner radius and 60% of the sensors are distributed along the outer radius) is found to have the best estimation accuracy compared to the other two sub-configurations (50% - 50% and 60% - 40% distributions, respectively). It is observed that the closer the inner radius approaches the outer radius and/or the lower the innerouter radius' sensor ratio, the better the estimation accuracy. It is thus recommended that all sensors should be distributed along the outer radius for better estimation accuracy. These findings would help direction finders such as engineers to economically utilize a given number of sensors.

**Key terms:** Array Signal Processing, Direction Finding, Planar Concentric Arrays, Circular Arrays, Estimation Accuracy, Parameter Estimation, Cramer-Rao Bound.

#### Introduction

Direction finding (DF) is also termed as direction-of-arrival (DoA) estimation problem. It basically refers to the problem of estimating angles-of-arrival (AoA) of an incident signal from an emitter (for instance plane wave or multiple plane waves) [1]. DF is a crucial technique in array signal processing following its wide-spread fields of applications especially in engineering. Some application areas include: radar, sonar, wireless communication, medical diagnosis and treatment, electronic surveillance, radio astrology [2]–[4], position location and tracing systems [5]. This is simply because it is a major method of location determination, in security services especially by reconnaissance of radio communications of criminal organization and in military intelligence by detecting activities of potential enemies and gaining information on enemy's communication order. Due to its diverse applications and difficulty in obtaining optimum estimator, the topic has attracted significant attention over the last several decades.

DF problem has so far been solved by employing various methods for both near-field and far-field sources emitting signal which is received by an array of sensors [6]. The methods aim to estimate the azimuth-polar angles-of-arrival. Some of the methods which have been employed in DF are: Maximum likelihood (ML) method [7], MUSIC (MUltiple SIgnal Classification) [8], ESPRIT (Estimation of Signal Parameters via Rotational Invariance Technique) [9], Cram´er-Rao Bound (CRB) [4], among other techniques. The Cram´er-Rao Bound which is utilized in this work has been found to be the most accurate technique in DF for it is the lowest error bound that any unbiased estimator can achieve and the simplest due to its simplicity in computations.

The aforementioned algorithms solve DF problem based on sensors either randomly distributed or arranged in a desired geometric pattern. The advantage of adopting any sensor-array geometry is mainly to improve the estimation performance. Among the many geometries that have been used in DF, circular and concentric circular geometries have a little bit more unique advantages which include: offering full rotational symmetry about the origin, flexibility in array pattern synthesis and design both in narrow band and broad band beam-forming applications, provision of almost invariant azimuth angle coverage and they can also yield invariant array pattern over a certain frequency band for beam-forming in 3-dimensions [17]–[21]. Concentric circular array geometries alone offer less mutual coupling effect due to their significant structure of the ring array [23], they yield smaller side lobes in beam-forming [22]–[26], provide higher angle resolution compared to uniform circular array geometries and requires less area for the same number of sensor elements [27] and they increase array's spatial aperture [17]–[21], [28], [29].

Despite the fact that the concentric circular arrays increase array's spatial aperture, the strategy in which the aperture is widened is a great concern as well as the number and the distribution of the sensors along the aperture. This now raises an important question that, how would the proportional variation of the inner radius while the outer radius is held constant affect the estimation accuracy of a 2-ring concentric planar array in direction finding? and how would varying the inner radius alone translate to sensors distribution on the inner-outer rings for the precision in direction finding? This work now proposed 3-configurations and their respective sub-configurations of a 2-ring concentric planar array which maintains all the advantages of concentric circular arrays and uses minimal number of sensors with an inter-spacing not exceeding half a wavelength. The three configurations are based on the proportional variation of the inner ring's radius as the outer ring's radius is held constant while the respective sub-configurations are based

on the distribution of sensors on the inner-outer rings in which the distributions are in 60%-40%, 50%-50% and 40%-60%. For the configuration one, the inner radius is a quarter of the outer radius, configuration two's radius is ahalf of the outer radius and configuration three's radius is three quarters of the outer radius. The sub-configurations use equal overall number of sensors (multiple of 4) but with 60%-40% distribution, 50%-50% distribution and 40%-60% distribution on the inner-outer rings respectively. The paper compares the estimation accuracy among the three configuration and their respective sub-configurations in DF via the derivation and analysis of their Cram´er-Rao bounds.

Finally, the paper consists of five sections in which Section I is the introduction, Section III presents the array response vector, Section III gives the Cram´er-Rao bound review and derivation, Section IV presents the Cram´er-Rao bound analysis for the 3-subconfiguration based on the sensors distribution, and Section V gives the conclusion.

# II Array Response Vector (ARV)

# II-A. Review Basics of ARV Using the General 2-Ring Concentric Planar array of Isotropic Sensors

Consider two concentric circles of radii  $R_{int}$  and  $R_{ext}$  sharing a common center at the Cartesian origin and lying on the x-y plane. See Figure 1.

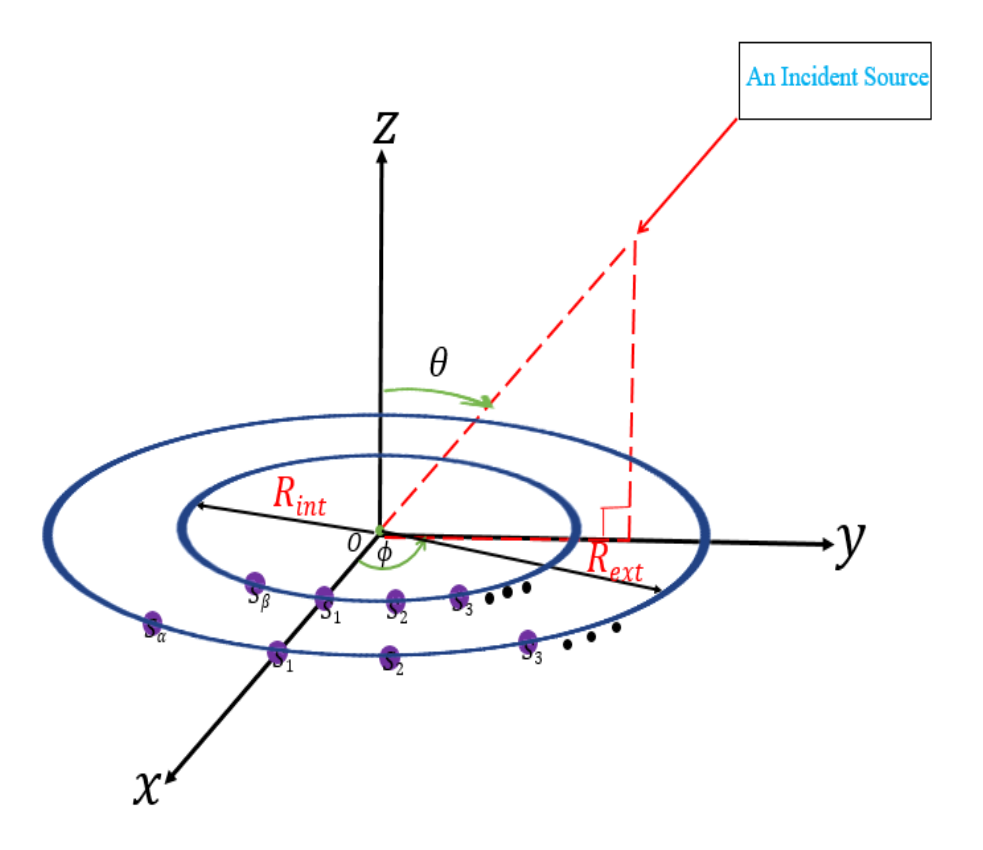


**Figure 1:** A general two-ring concentric planar array of isotropic sensors lying on the horizontal *x-y* plane and centered at the Cartesian origin.

The inner and the outer rings have  $L_{int}$  and  $L_{ext}$  number of isotropic sensors arranged on the rings' circumference respectively with equal inter-sensor spacing between any two adjacent sensors. The location of the  $\ell$ -th sensor in terms of the Cartesian coordinates equals

$$\boldsymbol{p}_{\ell} = \begin{cases} \left[ R_{int} cos \frac{2\pi(\ell_{int}-1)}{L_{int}}, R_{int} sin \frac{2\pi(\ell_{int}-1)}{L_{int}}, 0 \right]^{T}, & 1 \leq \ell_{int} \leq L_{int} \\ \left[ R_{ext} cos \frac{2\pi(\ell_{ext}-1)}{L_{ext}}, R_{int} sin \frac{2\pi(\ell_{ext}-1)}{L_{ext}}, 0 \right]^{T}, & 1 \leq \ell_{ext} \leq L_{ext} \end{cases}$$

$$(1)$$

where <sup>T</sup> denotes the transposition.

Consider an incident signal from a far-field emitter impinging on the origin at a polar-azimuth angles-of-arrival of  $\theta - \phi$  where  $\theta \in (0,\pi)$  and  $\phi \in (0,2\pi)$ . Then, the 2-ring's array response vector equals

$$a(\theta, \phi) = \begin{bmatrix} a_{int}(\theta, \phi) \\ a_{ext}(\theta, \phi) \end{bmatrix}, \tag{2}$$

where the  $\ell$ -th entries for  $a_{int}$  and  $a_{ext}$  are respectively given as:

$$[\mathbf{a}_{int}(\theta,\phi)]_{\ell} = exp\left\{j\frac{2\pi R_{int}}{\lambda}sin(\theta)cos\left(\phi - \frac{2\pi(\ell_{int}-1)}{L_{int}}\right)\right\}$$
(3)

For  $\ell_{int} = 1,2, \cdots L_{int}$  and

$$[\mathbf{a}_{ext}(\theta,\phi)]_{\ell} = exp\left\{j\frac{2\pi R_{ext}}{\lambda}sin(\theta)cos\left(\phi - \frac{2\pi(\ell_{ext}-1)}{L_{ext}}\right)\right\} \tag{4}$$

for  $\ell_{ext} = 1,2, \dots L_{ext}$ . In the above entries,  $\lambda$  is the wavelength of the incident signal.

### II-B. ARV of the Proposed 3-Configurations of the 2-Ring Concentric Planar Array

The 3-configurations of the 2-ring concentric planar array proposed in this work is based on the variation of the inner ring's radius in relation to the outer ring's radius while holding the latter radius constant. In all the configurations, the outer radius is hereby taken as  $8\lambda$ . Consider the illustration of the configurations as follows:

*II-B.1.* **Configuration One (C-1):** This configuration has the following properties. See fig 2.

i. 
$$R_{ext} = 8\lambda$$

ii. 
$$R_{int} = \frac{1}{4}(R_{ext}) = 2\lambda$$

With reference to Eq.(3)- Eq.(4) in Eq.(2), the array response vector for the C-1 is given as

$$\boldsymbol{a}_{C-1}(\theta,\phi) = \begin{bmatrix} exp\left\{j4\pi sin(\theta)cos\left(\phi - \frac{2\pi(\ell_{int}-1)}{L_{int}}\right)\right\}, \ 1 \leq \ell_{int} \leq L_{int} \\ exp\left\{j16\pi sin(\theta)cos\left(\phi - \frac{2\pi(\ell_{ext}-1)}{L_{ext}}\right)\right\}, 1 \leq \ell_{ext} \leq L_{ext} \end{bmatrix}$$
(5)

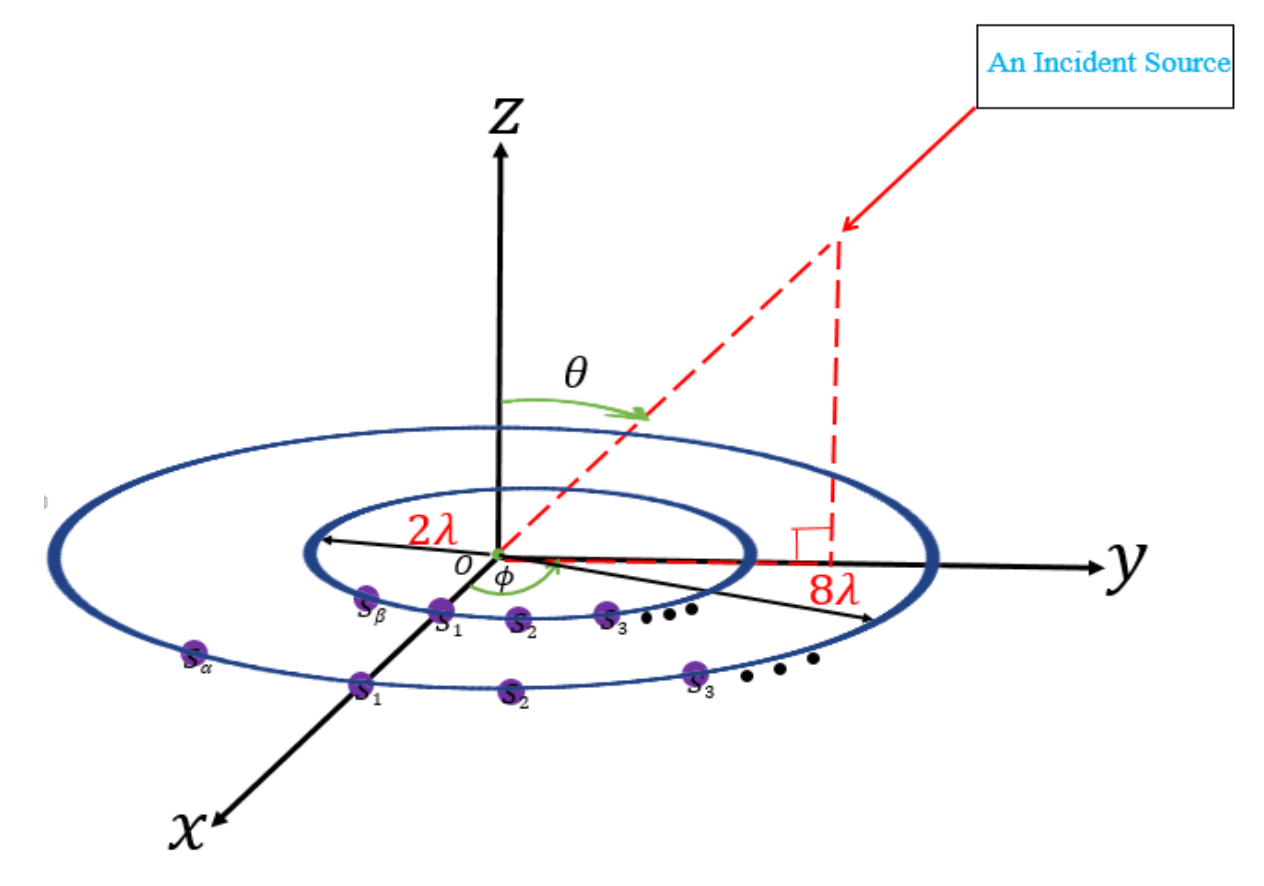


**Figure 2:** The proposed configuration one.  $\beta$  and  $\alpha$  symbolizes  $L_{int}$  and  $L_{ext}$  respectively.

*II-B.*2. Configuration Two (C-2): This configuration has the following properties.

i. 
$$R_{ext} = 8\lambda$$

ii. 
$$R_{int} = \frac{1}{2}(R_{ext}) = 4\lambda$$

Referring to Eq.(3)-Eq.(4) in Eq.(2), the array response vector for the C-2 equals

$$\boldsymbol{a}_{C-2}(\theta,\phi) = \begin{bmatrix} exp\left\{j8\pi sin(\theta)cos\left(\phi - \frac{2\pi(\ell_{int}-1)}{L_{int}}\right)\right\}, \ 1 \leq \ell_{int} \leq L_{int} \\ exp\left\{j16\pi sin(\theta)cos\left(\phi - \frac{2\pi(\ell_{ext}-1)}{L_{ext}}\right)\right\}, 1 \leq \ell_{ext} \leq L_{ext} \end{bmatrix}$$
(6)

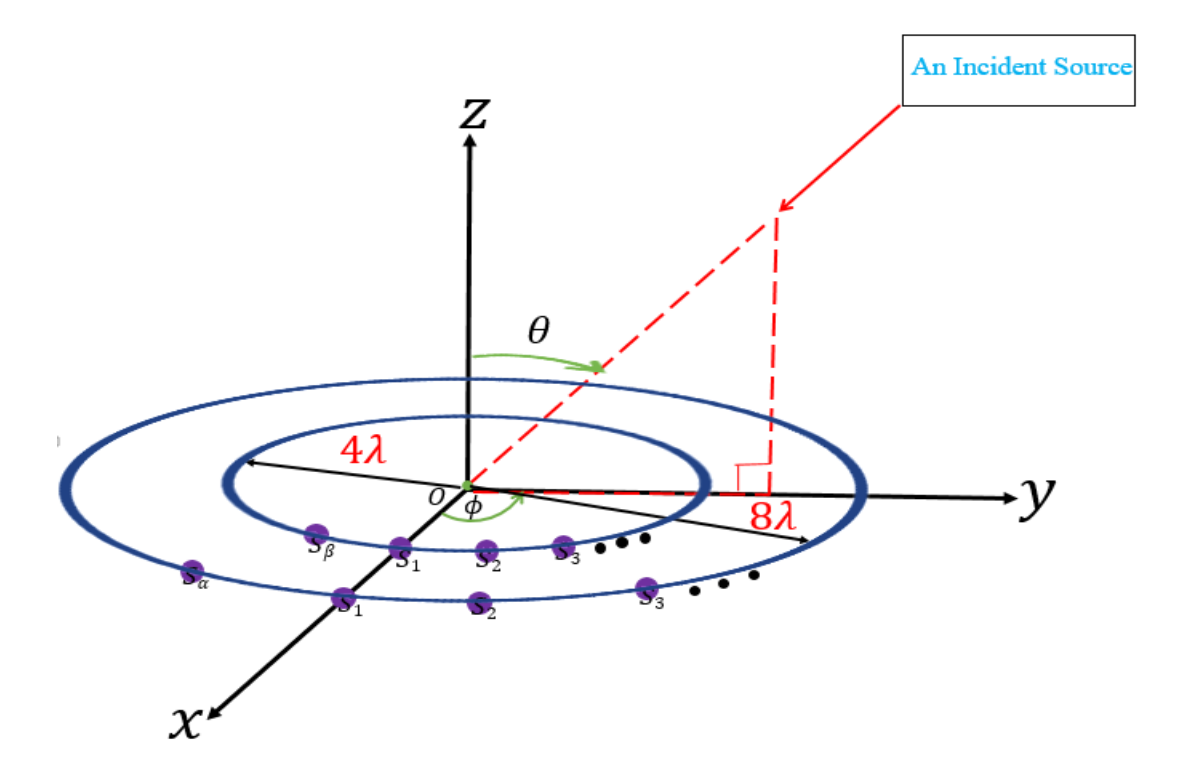


**Figure 3**: The proposed configuration two.  $\beta$  and  $\alpha$  symbolizes  $L_{int}$  and  $L_{ext}$  respectively

*II-B.3.* **Configuration Three (C-3):** This configuration has the following properties. See fig. 4.

i. 
$$R_{ext} = 8\lambda$$

ii. 
$$R_{int} = \frac{1}{2}(R_{ext}) = 6\lambda$$

With reference to Eq.(3)-Eq.(4) in Eq.(2), the array response vector for the C-3 equals

$$\boldsymbol{a}_{C-3}(\theta,\phi) = \begin{bmatrix} exp\left\{j12\pi sin(\theta)cos\left(\phi - \frac{2\pi(\ell_{int}-1)}{L_{int}}\right)\right\}, & 1 \leq \ell_{int} \leq L_{int} \\ exp\left\{j16\pi sin(\theta)cos\left(\phi - \frac{2\pi(\ell_{ext}-1)}{L_{ext}}\right)\right\}, & 1 \leq \ell_{ext} \leq L_{ext} \end{bmatrix}$$
(7)

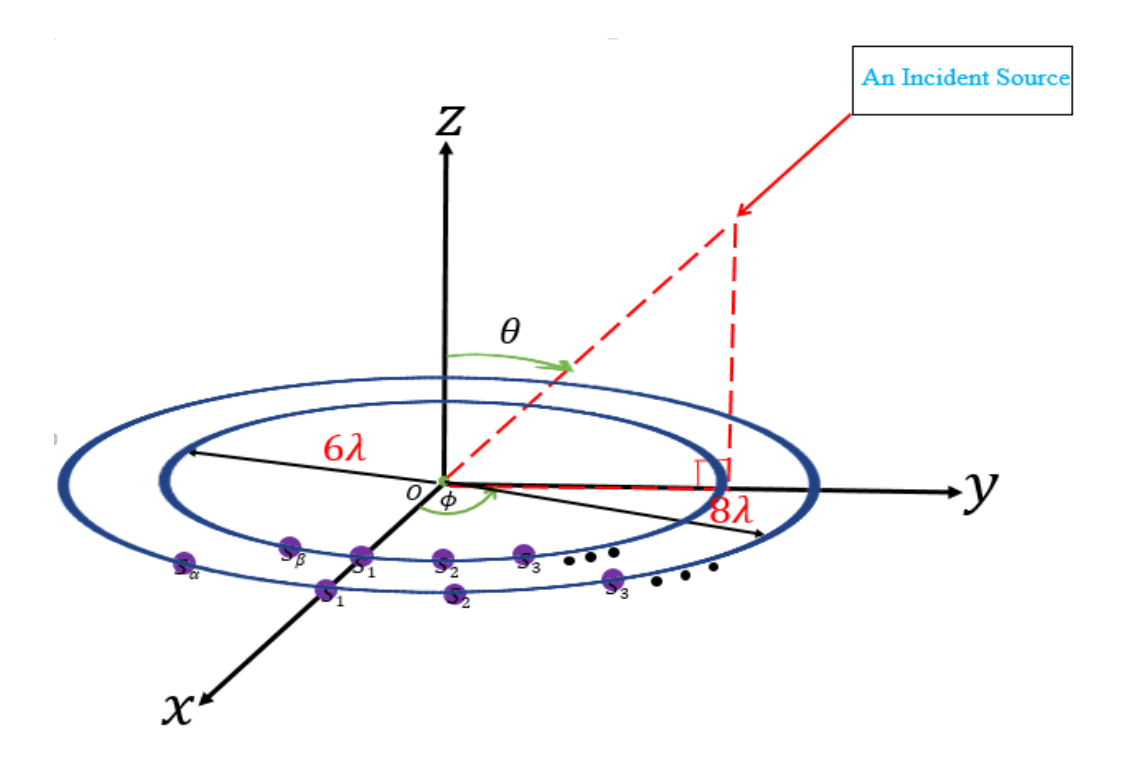


**Figure 4:** The proposed configuration three.  $\beta$  and  $\alpha$  symbolizes  $L_{int}$  and  $L_{ext}$  respectively.

#### III The Cram'er-Rao Bound Review and Derivation

### III-A. The Statistical Data Model

Let's consider a simple noise-corrupted replica of collected dataset at time instant *m* given by

$$\mathbf{z}(m) = \mathbf{a}(\theta, \phi)s(m) + \mathbf{n}(m) \tag{8}$$

where  $\mathbf{n}(m)$  is modeled as a complex-valued zero-mean additive white Gaussian noise (AWGN) with a prior known variance of  $\sigma_n^2$ , and s(m) is a scalar incident signal modeled as a white Gaussian complex-valued with a prior known variance of  $\sigma_s^2$  [1], [6], [10], [12]–[16], [18]. Then, for multiple-discrete-time instances M, the dataset is represented as

$$\check{\mathbf{z}} := [\{\mathbf{z}(1)\}^T, \{\mathbf{z}(2)\}^T, \cdots, \{\mathbf{z}(M)\}^T]^T = \mathbf{s} \otimes \mathbf{a}(\theta, \phi) + \check{\mathbf{n}}$$
(9)

where superscript  $^T$  denotes transposition,  $\otimes$  denotes the Kronecker product [12], [15] and

$$s := [s(1), s(2), \cdots, s(M)]^T$$

$$\check{\boldsymbol{n}} := [\{\boldsymbol{n}(1)\}^T, \{\boldsymbol{n}(2)\}^T, \cdots, \{\boldsymbol{n}(M)\}^T]^T.$$

#### III-B. The Fisher Information Matrix

The Fisher information matrix measures the amount of information that an observable random variable carries about an unknown parameter [31], [32]. Suppose the two parameters to-be-estimated are collected as entries of the  $2 \times 1$  vector  $\xi \in [\theta, \phi]$ . Then the Fisher information matrix (FIM)  $F(\xi)$  has a (k,r)th entry equal to (see (3.8) on page 72 of [30])

$$[F(\xi)]_{k,r} = 2Re\left\{ \left[ \frac{\partial \mu}{\partial \xi_k} \right]^H \Gamma^{-1} \frac{\partial \mu}{\partial \xi_r} \right\} + Tr\left\{ \Gamma^{-1} \left[ \frac{\partial \Gamma}{\partial \xi_k} \right]^H \Gamma^{-1} \frac{\partial \Gamma}{\partial \xi_r} \right\}$$
(10)

where  $Re\{\cdot\}$  signifies the real-value part of the entity inside the curly brackets,  $Tr\{\cdot\}$  denotes the trace of the entity inside the curly brackets, the superscript  $^H$  indicates conjugate transposition.

In equation (10),

$$\boldsymbol{\mu} \coloneqq E[\check{\mathbf{z}}] = \mathbf{s} \otimes \boldsymbol{a}(\theta, \phi) \tag{11}$$

$$\Gamma := E[(\check{\mathbf{z}} - \boldsymbol{\mu})(\check{\mathbf{z}} - \boldsymbol{\mu})^H] = \sigma_n^2 I_{(L_{int} + L_{ext})M}$$
(12)

are the mean and the covariance matrix of the data model where  $E[\cdot]$  represents the statistical expectation of the entity inside the square brackets and  $I_{(L_{int}+L_{ext})M}$  symbolizes an identity matrix of size  $(L_{int} + L_{ext})M$ . Clearly,  $\Gamma$  in Eq.(12) is functionally *in*dependent of both  $\theta$  and  $\phi$ , and thus the second term of (10) equals zero. Hence Eq.(10) reduces to

$$[F(\xi)]_{k,r} = \frac{2}{\sigma_s^2} Re \left\{ \left[ \frac{\partial \boldsymbol{\mu}}{\partial \xi_k} \right]^H \frac{\partial \boldsymbol{\mu}}{\partial \xi_r} \right\}$$

Where

$$\begin{bmatrix} \frac{\partial \boldsymbol{\mu}}{\partial \boldsymbol{\xi}_{k}} \end{bmatrix}^{H} \frac{\partial \boldsymbol{\mu}}{\partial \boldsymbol{\xi}_{r}} = \left[ \boldsymbol{s} \otimes \frac{\partial \boldsymbol{a}(\theta, \phi)}{\partial \boldsymbol{\xi}_{k}} \right]^{H} \left[ \boldsymbol{s} \otimes \frac{\partial \boldsymbol{a}(\theta, \phi)}{\partial \boldsymbol{\xi}_{r}} \right] \\
= \underbrace{\boldsymbol{s}^{H} \boldsymbol{s}}_{:=M\sigma_{s}^{2}} \otimes \left\{ \left[ \frac{\partial \boldsymbol{a}(\theta, \phi)}{\partial \boldsymbol{\xi}_{k}} \right]^{H} \left[ \frac{\partial \boldsymbol{a}(\theta, \phi)}{\partial \boldsymbol{\xi}_{r}} \right] \right\} \\
= M\sigma_{s}^{2} \left[ \frac{\partial \boldsymbol{a}(\theta, \phi)}{\partial \boldsymbol{\xi}_{k}} \right]^{H} \left[ \frac{\partial \boldsymbol{a}(\theta, \phi)}{\partial \boldsymbol{\xi}_{r}} \right].$$

Hence,

$$[\mathbf{F}(\boldsymbol{\xi})]_{k,r} = 2\mathbf{M} \frac{\sigma_s^2}{\sigma_n^2} Re \left\{ \left[ \frac{\partial \mathbf{a}(\theta, \phi)}{\partial \xi_k} \right]^H \left[ \frac{\partial \mathbf{a}(\theta, \phi)}{\partial \xi_r} \right] \right\}. \tag{13}$$

The Fisher information matrix equals

$$F(\xi) = \begin{bmatrix} F_{\theta,\theta} & F_{\theta,\phi} \\ F_{\phi,\theta} & F_{\phi,\phi} \end{bmatrix},$$

the inverse of which gives Cram´er-Rao bound of  $\theta$  and

φ:

$$\begin{bmatrix} CRB(\theta) & * \\ * & CRB(\phi) \end{bmatrix} = \begin{bmatrix} F_{\theta,\theta} & F_{\theta,\phi} \\ F_{\phi,\theta} & F_{\phi,\phi} \end{bmatrix}^{-1}$$
(14)

#### Iii-C. The Cram'Er-Rao Bound Derivation

Here we first derive the Cram´er-Rao bound for the general 2-ring concentric planar array then use the consequent results to give the Cram´er-Rao bounds for the 3-configurations. From Eq.(2), we have

$$\frac{\partial a(\theta,\phi)}{\partial \xi_k} = \left[ \left[ \frac{\partial a_{int}(\theta,\phi)}{\partial \xi_k} \right]^H, \left[ \frac{\partial a_{ext}(\theta,\phi)}{\partial \xi_k} \right]^H \right]^T, \tag{15}$$

where the  $\ell$ -th entries of  $\frac{\partial a_{int}(\theta,\phi)}{\partial \theta}$  and  $\frac{\partial a_{ext}(\theta,\phi)}{\partial \theta}$  for  $\ell_{int}=1,2,\cdots L_{int}$  and  $\ell_{ext}=1$ 

1,2,...  $L_{ext}$ , are respectively given by

$$\left[\frac{\partial a_{int}(\theta,\phi)}{\partial \theta}\right]_{\ell} = j2\pi \frac{R_{int}}{\lambda} cos(\theta) cos\left(\phi - 2\pi \frac{\ell_{int}-1}{L_{int}}\right) \times \boldsymbol{a}(\theta,\phi)$$
 (16)

and

$$\left[\frac{\partial a_{ext}(\theta,\phi)}{\partial \theta}\right]_{\ell} = j2\pi \frac{R_{ext}}{\lambda} \cos(\theta) \cos\left(\phi - 2\pi \frac{\ell_{ext}-1}{L_{ext}}\right) \times \boldsymbol{a}(\theta,\phi) \tag{17}$$

Similarly, the respective  $\ell$ -th entries of  $\frac{\partial a_{int}(\theta,\phi)}{\partial \phi}$  and  $\frac{\partial a_{ext}(\theta,\phi)}{\partial \phi}$  equals

$$\left[\frac{\partial a_{int}(\theta,\phi)}{\partial \phi}\right]_{\rho} = j2\pi \frac{R_{int}}{\lambda} cos(\theta) cos\left(\phi - 2\pi \frac{\ell_{int}-1}{L_{int}}\right) \times \boldsymbol{a}(\theta,\phi)$$
 (18)

and

$$\left[\frac{\partial a_{ext}(\theta,\phi)}{\partial \phi}\right]_{\ell} = j2\pi \frac{R_{ext}}{\lambda} cos(\theta) cos\left(\phi - 2\pi \frac{\ell_{ext}-1}{L_{ext}}\right) \times \boldsymbol{a}(\theta,\phi)$$
 (19)

From Eq.(16)-Eq.(17),

$$\left[\frac{\partial \boldsymbol{a}(\theta,\phi)}{\partial \theta}\right]^{H} \frac{\partial \boldsymbol{a}(\theta,\phi)}{\partial \theta} \\
= \left(2\pi \frac{R_{int}}{\lambda} \cos(\theta)\right)^{2} \underbrace{\sum_{\ell_{int}=1}^{L_{int}} \cos^{2}\left(\phi - 2\pi \frac{\ell_{int}-1}{L_{int}}\right)}_{L_{int}/2} \\
+ \left(2\pi \frac{R_{ext}}{\lambda} \cos(\theta)\right)^{2} \underbrace{\sum_{\ell_{ext}=1}^{L_{ext}} \cos^{2}\left(\phi - 2\pi \frac{\ell_{ext}-1}{L_{ext}}\right)}_{L_{ext}/2} \\
= \left(2\pi \frac{R_{int}}{\lambda} \cos(\theta)\right)^{2} \underbrace{\frac{L_{int}}{2} + \left(2\pi \frac{R_{ext}}{\lambda} \cos(\theta)\right)^{2} \frac{L_{ext}}{2}}_{L_{ext}} (20)$$

From Eq. (18)-Eq. (19),

$$\left[\frac{\partial \boldsymbol{a}(\theta,\phi)}{\partial \phi}\right]^{H} \frac{\partial \boldsymbol{a}(\theta,\phi)}{\partial \phi} \\
= \left(2\pi \frac{R_{int}}{\lambda} \sin(\theta)\right)^{2} \underbrace{\sum_{\ell=int}^{L_{int}} \sin^{2}\left(\phi - 2\pi \frac{\ell_{int} - 1}{L_{int}}\right)}_{L_{int}/2} \\
+ \left(2\pi \frac{R_{ext}}{\lambda} \sin(\theta)\right)^{2} \underbrace{\sum_{\ell=int}^{L_{ext}} \sin^{2}\left(\phi - 2\pi \frac{\ell_{ext} - 1}{L_{ext}}\right)}_{L_{ext}/2} \\
= \left(2\pi \frac{R_{int}}{\lambda} \sin(\theta)\right)^{2} \underbrace{L_{int}}_{L_{ext}/2} + \left(2\pi \frac{R_{ext}}{\lambda} \sin(\theta)\right)^{2} \underbrace{L_{ext}}_{L_{ext}/2} (21)$$

From Eq. (16) and Eq.(19),

$$\left[\frac{\partial a(\theta,\phi)}{\partial \theta}\right]^{H} \frac{\partial a(\theta,\phi)}{\partial \phi} = \left(2\pi \frac{R_{int}}{\lambda}\right)^{2} \frac{\sin(2\theta)}{4} \underbrace{\sum_{\ell_{int}=1}^{L_{int}} \sin\left(2\phi - 2\pi \frac{\ell_{int}-1}{L_{int}}\right)}_{0} + \left(2\pi \frac{R_{ext}}{\lambda}\right)^{2} \frac{\sin(2\theta)}{4} \underbrace{\sum_{\ell_{ext}=1}^{L_{ext}} \sin\left(2\phi - 2\pi \frac{\ell_{ext}-1}{L_{ext}}\right)}_{0} = 0 \quad (22)$$

using Eq.(20)-Eq.(22) in Eq.(13), we have

$$F_{\theta,\theta} = 4M \left(\frac{\pi \sigma_s}{\lambda \sigma_n}\right)^2 \left(R_{int}^2 L_{int} + R_{ext}^2 L_{ext}\right) \cos^2(\theta)$$
 (23)

$$F_{\theta,\phi} = 0, \tag{24}$$

$$F_{\phi,\phi} = 4M \left(\frac{\pi}{\lambda} \frac{\sigma_s}{\sigma_n}\right)^2 \left(R_{int}^2 L_{int} + R_{ext}^2 L_{ext}\right) \sin^2(\theta). \tag{25}$$

Using Eq.(23)-Eq.(24) in Eq.(14), we have

$$CRB(\theta) = F_{\theta,\phi}^{-1} = \frac{1}{M} sec^{2}(\theta) \left[ \left( 2\pi \frac{R_{int}}{\lambda} \right)^{2} L_{int} + \left( 2\pi \frac{R_{ext}}{\lambda} \right)^{2} L_{ext} \right]^{-1} (26)$$

and

$$CRB(\phi) = F_{\phi,\phi}^{-1} = \frac{1}{M}csc^{2}(\theta) \left[ \left( 2\pi \frac{R_{int}}{\lambda} \right)^{2} L_{int} + \left( 2\pi \frac{R_{ext}}{\lambda} \right)^{2} L_{ext} \right]^{-1} (27)$$

# Consequently, the Cram´Er-Rao Bounds for the 3-Configurations are Given as Follows:

For the configuration one

$$CRB_{c-1}(\theta) = \frac{1}{M} \frac{1}{4\pi^2} sec^2(\theta) [4L_{int} + 64L_{ext}]^{-1} \left(\frac{\sigma_n}{\sigma_c}\right)^2$$
 (28)

and

$$CRB_{c-1}(\phi) = \frac{1}{M} \frac{1}{4\pi^2} csc^2(\theta) [4L_{int} + 64L_{ext}]^{-1} \left(\frac{\sigma_n}{\sigma_s}\right)^2$$
 (29)

For the configuration two

$$CRB_{c-2}(\theta) = \frac{1}{M} \frac{1}{4\pi^2} sec^2(\theta) [16L_{int} + 64L_{ext}]^{-1} \left(\frac{\sigma_n}{\sigma_s}\right)^2$$
 (30)

and

$$CRB_{c-2}(\phi) = \frac{1}{M} \frac{1}{4\pi^2} csc^2(\theta) [16L_{int} + 64L_{ext}]^{-1} \left(\frac{\sigma_n}{\sigma_s}\right)^2$$
 (31)

For the configuration three

$$CRB_{c-3}(\theta) = \frac{1}{M} \frac{1}{4\pi^2} sec^2(\theta) [36L_{int} + 64L_{ext}]^{-1} \left(\frac{\sigma_n}{\sigma_s}\right)^2$$
 (32)

and

$$CRB_{c-3}(\phi) = \frac{1}{M} \frac{1}{4\pi^2} csc^2(\theta) [36L_{int} + 64L_{ext}]^{-1} \left(\frac{\sigma_n}{\sigma_s}\right)^2$$
 (33)

**Observation**: Comparing Eq.(28)-Eq.(33), it is clear that since  $L_{int} < L_{ext}$ , the Cram´er-Rao bounds decreases with increase in the inner radius implying that the estimation accuracy (precision) increases as the inner radius approaches the outer radius.

# IV The Cram´er-Rao Bound Analysis for the 3-Sub-Configuration Based on the Sensors´ Distribution

These sub-configurations are based on the sensors distribution on the inner-outer rings while maintaining the overall number of sensors to be equal. The distributions are in 60% – 40%, 50% – 50% and 40%–60% of the overall number of sensors on the inner-outer rings respectively. For instance, consider the overall number of sensors to be 40.

# IV-A. Sub-Configuration One

This sub-configuration adopts 60% - 40% sensors distribution implying that the inner ring has 24 sensors while the outer ring has 16 sensors. i.e  $L_{int} = 24$  and  $L_{ext} = 16$ . Now inserting  $L_{int} = 24$  and  $L_{ext} = 16$  in Eq.(28)-Eq.(33), we have

$$(2\pi)^{2}M\left(\frac{\sigma_{s}}{\sigma_{n}}\right)^{2}\cos^{2}(\theta)CRB_{c-1}(\theta) \equiv (2\pi)^{2}M\left(\frac{\sigma_{s}}{\sigma_{n}}\right)^{2}\cos^{2}(\theta)CRB_{c-1}(\phi)$$
$$= [(4\times24) + (64\times16)]^{-1}$$
$$= [1120]^{-1} \tag{34}$$

$$(2\pi)^{2}M \left(\frac{\sigma_{s}}{\sigma_{n}}\right)^{2} \cos^{2}(\theta) CRB_{c-1}(\theta) \equiv (2\pi)^{2}M \left(\frac{\sigma_{s}}{\sigma_{n}}\right)^{2} \cos^{2}(\theta) CRB_{c-1}(\phi)$$

$$= [(16 \times 24) + (64 \times 16)]^{-1}$$

$$= [1408]^{-1}$$

$$(35)$$

$$(2\pi)^{2}M \left(\frac{\sigma_{s}}{\sigma_{n}}\right)^{2} \cos^{2}(\theta) CRB_{c-1}(\theta) \equiv (2\pi)^{2}M \left(\frac{\sigma_{s}}{\sigma_{n}}\right)^{2} \cos^{2}(\theta) CRB_{c-1}(\phi)$$

$$= [(36 \times 24) + (64 \times 16)]^{-1}$$

$$= [1888]^{-1}$$

$$(36)$$

# IV-B. Sub-Configuration Two

This sub-configuration adopts 50% – 50% sensors distribution implying that both the inner ring and the outer ring have equal number of sensors. i.e  $L_{int} = 20$  and  $L_{ext} = 20$ . Now inserting  $L_{int} = 20$  and  $L_{ext} = 20$  in Eq.(28)-Eq.(33), we have

$$(2\pi)^{2}M\left(\frac{\sigma_{s}}{\sigma_{n}}\right)^{2}\cos^{2}(\theta)CRB_{c-2}(\theta) \equiv (2\pi)^{2}M\left(\frac{\sigma_{s}}{\sigma_{n}}\right)^{2}\cos^{2}(\theta)CRB_{c-2}(\phi)$$

$$= [(4\times20) + (64\times20)]^{-1}$$

$$= [1360]^{-1}$$
(37)

$$(2\pi)^{2}M\left(\frac{\sigma_{s}}{\sigma_{n}}\right)^{2}\cos^{2}(\theta)CRB_{c-2}(\theta) \equiv (2\pi)^{2}M\left(\frac{\sigma_{s}}{\sigma_{n}}\right)^{2}\cos^{2}(\theta)CRB_{c-2}(\phi)$$
$$= [(16\times20) + (64\times20)]^{-1}$$
$$= [1600]^{-1} \tag{38}$$

$$(2\pi)^{2}M \left(\frac{\sigma_{s}}{\sigma_{n}}\right)^{2} \cos^{2}(\theta) CRB_{c-2}(\theta) \equiv (2\pi)^{2}M \left(\frac{\sigma_{s}}{\sigma_{n}}\right)^{2} \cos^{2}(\theta) CRB_{c-2}(\phi)$$

$$= [(36 \times 20) + (64 \times 20)]^{-1}$$

$$= [2000]^{-1}$$
(39)

# IV-C. Sub-Configuration Three

This sub-configuration adopts 40% - 60% sensors distribution implying that the inner ring has 16 sensors while the outer ring has 24 sensors. i.e  $L_{int} = 16$  and  $L_{ext} = 24$ . Now inserting  $L_{int} = 16$  and  $L_{ext} = 24$  in Eq.(28)-Eq.(33), we have

$$(2\pi)^{2}M\left(\frac{\sigma_{s}}{\sigma_{n}}\right)^{2}\cos^{2}(\theta)CRB_{c-3}(\theta) \equiv (2\pi)^{2}M\left(\frac{\sigma_{s}}{\sigma_{n}}\right)^{2}\cos^{2}(\theta)CRB_{c-3}(\phi)$$

$$= [(4\times16) + (64\times24)]^{-1}$$

$$= [1600]^{-1} \qquad (40)$$

$$(2\pi)^{2}M\left(\frac{\sigma_{s}}{\sigma_{n}}\right)^{2}\cos^{2}(\theta)CRB_{c-3}(\theta) \equiv (2\pi)^{2}M\left(\frac{\sigma_{s}}{\sigma_{n}}\right)^{2}\cos^{2}(\theta)CRB_{c-3}(\phi)$$

$$= [(16\times16) + (64\times24)]^{-1}$$

$$= [1792]^{-1} \qquad (41)$$

$$(2\pi)^{2}M\left(\frac{\sigma_{s}}{\sigma_{n}}\right)^{2}\cos^{2}(\theta)CRB_{c-3}(\theta) \equiv (2\pi)^{2}M\left(\frac{\sigma_{s}}{\sigma_{n}}\right)^{2}\cos^{2}(\theta)CRB_{c-3}(\phi)$$

$$= [(36 \times 16) + (64 \times 24)]^{-1}$$

$$= [2112]^{-1} \tag{42}$$

**Observation**: From Eq.(34)-Eq.(42), it is clear that, the Cram´er-Rao bounds decreases as the inner radius approaches the outer radius across all the sub-configurations. However, configuration three has the lowest Cram´er-Rao bounds in all the sub-configurations and hence has the best estimation accuracy among the proposed configurations of the 2-ring concentric planar array.

#### Conclusion

Three configurations of a 2-ring concentric planar array with their respective sub-configurations are proposed. The configurations are based on the variation of the inner ring's radius as the outer ring's radius is held constant while the respective sub-configurations are based on the distribution of sensors on the inner-outer rings in which the distributions are in 60% – 40%, 50% – 50% and 40% – 60%. The comparison of the estimation accuracy for the aforementioned configurations and their respective sub-configurations in direction finding is verified via the Cram´ er-Rao bound derivation and analysis. It has been observed that the Cram´ er-Rao bound decreases as the inner radius approaches the outer radius and the configuration three has the lowest Cram´ er-Rao bound across all the sub-configurations. Thus among the proposed configurations of the 2-ring concentric planar array, configuration three has the best estimation accuracy (precision) in direction finding. Observations from this study would greatly help engineers to economically utilize a given number of sensors and hence minimizing hardware cost.

#### References

Abedin. M.J & Mohan, A.S. (2010). Maximum Likelihood Near Field Localisation Using Concentric Circular Ring Array. *IEEE International Conference on in Electromagnetics in Advanced Applications*, pp. 533-536.

Albagory, Y.A M. Dessouky, M & Sharshar, H (2007). An Approach for Low Sidelobe Beamforming in Uniform Concentric Circular Arrays, *Wireless Personal Communications*, vol. 43, no. 4, pp. 1363-1368.

Ata, S.O & Isik, C. (2013). High-Resolution Direction-of-Arrival Estimation via Concentric Circular Arrays, *ISRN Signal Processing*, March, 2013.

Castanie, F. (2011). *Digital spectral analysis: Parametric, non-parametric and advanced methods*, New York, New York, U.S.A.: John Wiley and Sons.

Das, R (1966). Concentric ring array," *IEEE Transactions on Antennas and Propagation*, vol. 14, no. 3, pp. 398-400.

Delmas, J.P, M. Korso, M.N., Gazzah, H & Castella, M. (2016). CRB Analysis of Planar Antenna Arrays for Optimizing Near-Field Source Localization, *Signal Processing*, Vol. 127, pp. 117-134.

Delmas, J.P. & Gazzah, H (2013). CRB Analysis of Near-Field Source Localization Using Uniform Circular Arrays, *IEEE International Conference on Acoustics, Speech and Signal Processing*, pp. 3996-4000.

Devendra, M & Manjunathachari, K (2015). Solar DC Microgrid for Rural Electrification: A Case Study," *International Advanced Research Journal in Science, Engineering and Technology (IARJSET)*, Vol. 2, No. 1, pp. 1-5.

Friedlander, B (2009). Wireless direction-finding fundamentals in classical and modern direction-of-arrival estimation, pp. 1-51, Elsevier

Haupt, R.L. (2008). Optimized element spacing for low sidelobe concentric ring arrays, *IEEE Transactions on Antennas and Propagation*, vol. 56, no. 1, pp. 266-268.

Jiang, Y. & Zhang, S. (2013). An Innovative Strategy for Synthesis of Uniformly Weighted Circular Aperture Antenna Array Based on the Weighting Density Method, *IEEE Antennas and Wireless Propagation Letters*, vol. 12, pp. 725-728, May 2013.

Kajaree, D & Behera, R (2017). A Survey on Web Crawler Approaches, *International Journal of Innovative Research in Computer and Communication Engineering*, vol. 5, no. 2, pp. 1302-1309.

Kay, S.M (1993). Fundamental of Statistical Signal Processing: Estimation Theory, Upper Saddle River, New Jersey, USA: Prentice Hall.

Kitavi, D.M (2016). Direction finding with the sensors' gains suffering Bayesian uncertainty - hybrid CRB and MAP estimation," *IEEE Transactions on Aerospace and Electronic Systems*, vol. 52, no. 4, pp. 2038-2044.

Kitavi, D.M. (2016). Direction Finding with The Sensors' Gains Suffering Bayesian Uncertainty - Hybrid CRB and MAP Estimation," *IEEE Transactions on Aerospace and Electronic Systems*, Vol. 52, No. 4, pp. 2038-2044.

Kitavi, D.M. Wong, K. T & Hung, C (2017). An L-shaped array with nonorthogonal axesits 2 Cramer-Rao bound for direction finding," *IEEE Transactions on Aerospace and Electronic Systems*, vol. 54, no. 1, pp. 486-492.

Kitavi, T. C (2016). A Tetrahedral Array of Isotropic Sensors, Each Suffering a Random Complex Gain -The Resulting Hybrid Cramr-Rao Bound for Direction Finding," *Proceedings of the IEEE National Aerospace Electronics Conference*, NAECON, pp. 412-415.

Krishnaveni, V & T. Kesavamurthy, T (2013). Beamforming for Direction-of-Arrival (DOA) estimation-A survey," *International Journal of Computer Applications*, vo. 61, no. 11, pp. 975-8887.

Mendez, R.A, Silva, J.F, Orsotica, R R. & Lobos, R. (2014). Analysis of the Cramer-Rao Lower Uncertainty Bound *In* the Joint Estimation Of Astrometry and Photometry," *Publications of the Astronomical Society of the Pacific*, vol. 126, no. 942, pp. 798-810, 2014.

Ram, G. Mandal, D., Kar, R & Ghoshal, S.P. (2015). Circular and Concentric Circular Antenna Array Synthesis Using Cat Swarm Optimization," *IETE Technical Review*, Vol. 32, no. 3, pp. 204-217.

Sasaki, Y. Tamai, S. Kagami, S. & Mizoguchi, H. (2005). 2D Sound Source Localization on a Mobile Robot with a Concentric Microphone Array, *IEEE International Conference on Systems, Man and Cybernetics*, vol. 4, pp. 3528-3533.

Shavit, R. Pazin, L, Israeli, Y. Sigalov, M & Leviatan, Y. (2005). Dual Frequency and Dual Circular Polarization Microstrip Nonresonant Array Pin-Fed from a Radial Line, *IEEE Transactions on Antennas and Propagation*, Vol. 53, no. 12, pp. 38973905.

Tayem, N& Kwon, H.M (2005). L-Shape 2-Dimensional Arrival Angle Estimation with Propagator Method," *IEEE Transactions on Antennas and Propagation*, Vol. 53, no. 5, pp. 1622-1630.

Van Trees, H.L (2002). *Detection, Estimation and Modulation Theory, Part IV: Optimum Array Processing*. New York: John Wiley and Sons.

Vorobyov, S. A. Gershman, B & Wong, K.M (2005). Maximum Likelihood Direction-of-Arrival Estimation *In* Unknown Noise Fields Using Sparse Sensor Arrays," *IEEE Transactions on Signal Processing*, vol. 53, no. 1, pp. 34-43.

Vu, D. T, Renaux, A. Boyer, R & Marcos, S. (2013). A Cramr Rao Bounds Based Analysis of 3D Antenna Array Geometries Made from ULA Branches," *Multidimensional Systems and Signal Processing*, Vol. 24, no. 1, pp. 121-155.

Wang, L. Wang, G & Chen, Z. (2013). Joint DOA-Polarization Estimation based on Uniform Concentric Circular Array, *Journal of Electromagnetic Waves and Applications*, vol. 27, no. 13, pp. 1702-1714.

Wong, K.T & Zoltowski, M.D. (2000). Self-Initiating MUSIC-based Direction Finding and Polarization Estimation *In* Spatio-Polarizational Beamspace, *IEEE Transactions on Antennas and Propagation*, vol. 48, no. 8, pp. 1235-1245.

Zhang, L. Jiao, Y.C, Chen, B & Weng, Z. B. (2012). Design of Wideband Concentric-Ring Arrays with Three-Dimensional Beam Scanning Based on the Optimization of Array Geometry, *Electromagnetics*, Vol. 32, no. 6, pp. 305-320.

Zhao, X, Yang, Q, & Zhang, Y. (2016). A Hybrid Method for the Optimal Synthesis of 3-D Patterns of Sparse Concentric Ring Arrays, *IEEE Transactions on Antennas and Propagation*, Vol. 64, no. 2, pp. 515-524.

Zhao, X, Zhang, Y & Yang, Q. (2017). Synthesis of Sparse Concentric Ring Arrays Based on Bessel Function, *IET Microwaves, Antennas and Propagation*, Vol. 11, no. 11, pp. 1651-1660.

Zoltowski, M. D & Wong, K.T. (2000). ESPRIT-Based 2-D Direction Finding with a Sparse Uniform Array of Electromagnetic Vector Sensors," *IEEE Transactions on Signal Processing*, vol. 48, no. 8, pp. 2195-2204, August 2000.